Chemical Engineering Journal 463 (2023) 142345

Contents lists available at ScienceDirect

Chemical Engineering Journal

journal homepage: www.elsevier.com/locate/cej

Enhanced photocatalytic degradation of organic contaminants in water by highly tunable surface microlenses

Qiuyun Lu [a], Lingling Yang [b], Pamela Chelme-Ayala [b], Yanan Li [a], Xuehua Zhang [a,*], Mohamed Gamal El-Din [b,*]

[a] *Department of Chemical and Materials Engineering, University of Alberta, 9211 116 Street NW, Edmonton, Alberta, T6G 1H9, Canada*
[b] *Department of Civil and Environmental Engineering, University of Alberta, 9211 116 Street NW, Edmonton, Alberta, T6G 1H9, Canada*

ARTICLE INFO

Keywords:
Surface microlenses
Microlens array
Focus effect
Photocatalysis
Water decontamination

ABSTRACT

Photocatalysis is one of the dominant technologies used to enhance the efficiency of water decontamination with light-based treatments. However, the effectiveness of photocatalysts is usually limited by the irradiation conditions and the properties of the water matrix. In this work, we have demonstrated the capability of surface microlenses (MLs) as a clean technology for more efficient photocatalytic water decontamination. Random or ordered surface MLs were fabricated from simple polymerization of nanodroplets produced in a solvent exchange process. Both random microlenses (MLR) and microlenses array (MLA) could enhance the photocatalytic degradation efficiency (η) of four representative organic pollutants, including methyl orange (MO), norfloxacin (NFX), sulfadiazine (SFD), sulfamethoxazole (SMX), spiked in ultra-pure water, synthetic natural water, or real river water. By controlling the conditions of light treatment, η could be enhanced by up to 402%. The effectiveness of surface MLs was validated under both visible LED light and simulated solar light and for two photocatalysts zinc oxide (ZnO) and titanium dioxide (TiO_2). By reducing the concentration of the photocatalysts from 100 to 5 mg/L and the intensity of irradiation intensity from 1 Sun to 0.3 Sun, our findings suggest that the enhancement factor by MLs was higher at lower catalyst concentration, or at lower light intensity. Based on optical simulations and experimental results, we demonstrated that surface MLs optimize the light distribution and promote the formation of active species, which results in the enhancement of η. The use of MLs may serve as a novel strategy to improve the photocatalytic degradation of micropollutants, especially in places where the available light source is weak, such as indoors or in cloudy regions.

Synopsis: MLs-enhanced photocatalysis degradation of organic contaminants in different water matrices.

1. Introduction

Photoreactions are widely applied in different fields [1], such as data storage [2,3], display [4], light generation [5,6], polymerization [7,8], and light-driven degradation [9,10]. Many clean-energy technologies for water treatment benefits from photoreactions [11]. For instance, solar-based water disinfection utilizes solar energy to inactivate or eliminate pathogenic contaminants in water with portable containers, which is a low-cost and convenient method to provide safe household water [12,13]. In many types of photoreactions [14], photocatalysis, which is the photoreactions accelerated by photocatalysts, is one of the dominant technologies to remove the organic micropollutants in natural water [15–17]. The most common type of photocatalysis in water treatment is heterogeneous photocatalysis with semiconductor materials, such as titanium dioxide (TiO_2) [18] and zinc oxide (ZnO) [19]. The band gap of ZnO and TiO_2 can be narrowed and be responsive to visible light [20,21]. For example, the energy gap of ZnO reached 2.85 eV, [22] while a TiO_2-based catalyst had a band gap around 2.00 eV [23]. The action spectra of ZnO and TiO_2 also confirmed their response under visible light and solar light [24–26]. However, the application of photoreactions is often limited due to the inefficient utilization of light [27].

One of the main reasons that restrict the development of solar-driven photocatalytic degradation of organic pollutants in the aqueous environment is the instability of solar light under different scenarios [28,29]. For example, sunlight is attenuated when the wastewater has high turbidity [30] or when the rainy and cloudy weather appears [31]. As a result, the number of photons that can be absorbed into the system decreases, so the activity of photocatalysts is considerably inhibited. In order to maximize the potential of photocatalysts under insufficient

---

[*] Corresponding author.
E-mail addresses: xuehua.zhang@ualberta.ca (X. Zhang), mgamalel-din@ualberta.ca (M. Gamal El-Din).

https://doi.org/10.1016/j.cej.2023.142345
Received 8 November 2022; Received in revised form 19 February 2023; Accepted 6 March 2023

light, strategies to increase the number of species undergoing a photochemical process with a given amount of photons are needed. Several strategies have been widely investigated for this purpose, including incorporating light engineering design in photoreactors to improve their performance [32,33], establishing a flow reactor to enhance the mass transfer or to shorten the light path [34], and preparing engineering photocatalytic materials for more efficient photocatalysis [35]. Introducing lenses into photoreaction systems is a potential alternative because of the ability of lenses to redistribute light [36]. The focusing effect of a lens creates high local light intensity at the focal point, accelerating the local photoreaction rates.

Surface microlenses (MLs) are novel lenses with small dimensions and a large number fabricated on a solid surface [37,38]. There are several advantages from surface MLs in a photoreaction process. First of all, surface MLs can be integrated into various reactors due to their small dimensions [39,40]. Besides, such lenses have short focal distances with strong near-field focusing effect [41,42]. Last but not the least, the MLs with well-controlled optical properties and good durability can be prepared and flexibly modified by various methods [43,44]. Commonly used fabrication methods include laser writing [45,46], hot embossing [47,48], soft lithography [49,50], and drop-templating [51,52]. The fabrication of surface MLs based on nanodroplet polymerization is one of the promising technologies that are highly tunable and affordable [53]. Through this method, surface nano-/microlenses are obtained after the polymerization of surface droplets formed in a solvent exchange [54]. Notably, the morphology and spatial arrangement of surface nano-/microlenses are tunable [55] with the method, and the functional components, such as plasmonic nanoparticles [42], can be introduced into the system conveniently.

In the work conducted by Dongare et al. [56], the feasibility of integrating lenses with light-driven membrane devices for water purification was demonstrated, where a higher energy conversion rate of the device was achieved because of the focus effect of lenses. On a smaller scale, the acceleration of the photoreactions by surface MLs was validated through the in-situ photoreduction of silver nitrate [42] and the direct photolysis of micropollutants [57]. Therefore, such surface MLs are also expected to be effective in enhancing the solar-driven photocatalytic degradation of contaminants in water. Implementing surface MLs based on the solvent exchange process as a candidate strategy for enhancing photodegradation efficiency under insufficient irradiation is worthy of investigation. However, the mechanisms of photocatalytic degradation combined with surface MLs have not been explored, so as the influence of the properties of MLs, photocatalysts, light sources, and water matrix on the degradation process.

In this work, we evaluated the performance of surface MLs in enhancing the photocatalytic degradation of four typical organic pollutants in river water, including methyl orange (MO), norfloxacin (NFX), sulfadiazine (SFD), and sulfamethoxazole (SMX) [58–60]. Surface MLs were photopolymerized from the nanodroplets obtained in a solvent exchange process [61] and could be flexibly tailored for better performance. The optimized spatial arrangement of surface MLs was selected based on the light treatment results. The mechanisms of surface MLs-assisted photocatalytic degradation were investigated with experiments and optical simulation. By tuning the light sources, irradiation intensity, water matrices, and the geometry of reactors, the practical conditions with limited irradiation were simulated where the influence of surface MLs on photocatalytic degradation efficiency is studied. Last but not the least, we used two commercial photocatalysts with good stability and durability [62,63], ZnO and TiO_2, to assess the applicability of surface MLs in varied catalytic processes. The capability of surface MLs in promoting the photocatalytic degradation of organic pollutants in water was validated.

2. Experimental section

2.1. Fabrication and characterization of random surface microlenses and high-curvature microlens array on planar glass substrates

Surface microlenses (MLs) were fabricated by photopolymerization of surface droplets under UV light, as shown in Fig. 1(a). The size and spatial distribution of surface MLs were determined by the diameters and positions of surface droplets. The solvent exchange process enabled us to flexibly control the formation of surface droplets and further adjust the properties of surface MLs [53,64]. In the solvent exchange process, a self-assembled chamber was filled with a solution (solution A) which was a mixture of monomer, photoinitiator, ethanol, and Milli Q water. Then, Milli Q water saturated with monomer and initiator (solution B) was inserted into the chamber at a fixed flow rate. Consequently, surface droplets composed of monomers and the photoinitiator formed on the substrates due to the oversaturation during the solvent exchange process. When the substrate was homogeneously hydrophobic, surface droplets grew and coalesced on the substrate, leading to the formation of surface MLs with non-uniform size and spatial distribution (random MLs, MLR) after UV curing. On the other hand, surface droplet arrays (MLAs) could be prepared on a pre-patterned substrate with ordered hydrophobic microdomains [55].

Random surface MLs (MLR) for photocatalytic degradation system were prepared using methyl methacrylate (MMA) (≥ 98.5%, Alfa Aesar) as the monomer and 2-hydroxy-2-methylpropiophenone (96%, Fisher) as the photoinitiator. Solution A was prepared by adding 8.0 vol% MMA and 0.8 vol% photoinitiator in 40 vol% ethanol aqueous solution. Then, Milli Q water saturated with MMA and photoinitiator, namely solution B, was injected into the chamber at a flow rate of 50 mL/h. A glass slide homogeneously hydrophobized with octadecyltrichlorosilane (OTS) (98.9%, Acros Organics, Fisher Scientific) was placed on top of the chamber as the substrate for surface droplets and MLs. The OTS coating of the substrate was prepared according to the procedure described by Zhang and Ducker [61]. The condition used to fabricate the random surface MLs was the optimized one in our previous work [57]. After the standard solvent exchange process, the chamber filled with liquid was sealed and horizontally set under UV light (365 nm, Analytik Jena UV lamp) for 15 min.

Surface ML arrays (MLAs) in the photodegradation processes were fabricated with lauryl methacrylate (LMA, Acros Organics) as the monomer in solution A. The solubility of LMA in water was lower than MMA, leading to more stable surface droplets during the solvent exchange and ensuring the uniformity of surface MLAs. The pre-patterned substrate used for droplet formation was decorated with circular hydrophobic microdomains arranged in an array, fabricated by a photolithography process on an OTS-coated glass slide [55]. The diameter of each circular domain was 5.0 μm, and the spacing between two adjacent domains was 2.5 μm. By repeating the process of solvent exchange and UV curing, MLAs with higher curvature could be achieved [65]. In this work, three rounds of solvent exchange-UV curing process were performed. Solution A for the solvent exchange process was prepared by adding LMA and the photoinitiator (1/10 volume of LMA) into ethanol, while solution B was the LMA and photoinitiator saturated water. The LMA concentration in solution A in the three rounds of solvent exchange was 2 vol%, 4 vol%, and 2 vol%, respectively, while the flow rate of adding solution B into solution A was 8 mL/h, 4 mL/h, and 4 mL/h, correspondingly. The UV curing step lasted for 15 min after each round of the solvent exchange process, after which the high-curvature poly(lauryl methacrylate) (PLMA) MLA were obtained. The curvature of the PLMA MLA could not further increase because the adjacent MLs would be connected if more LMA were added on top of the MLs base.

Surface random MLs and ML arrays were observed under an optical microscope equipped with a camera (Nikon H600l and Nikon DSFi3). The lateral size and surface coverage rate of MLs were calculated by

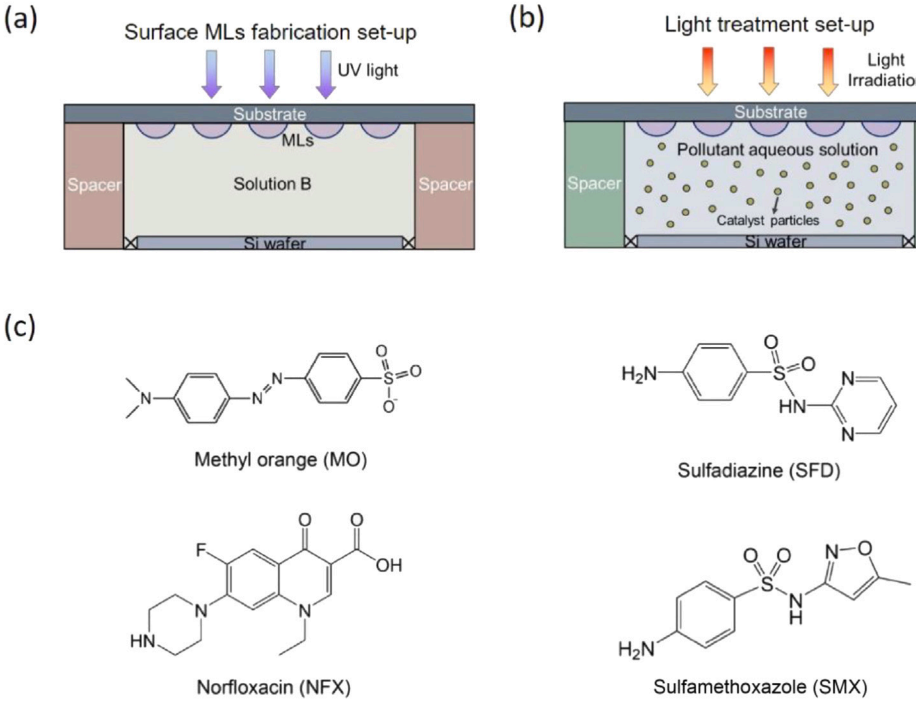

Fig. 1. (a) Sketch of the fabrication process of surface MLs. The chamber height is 0.57 mm, the width is 12.2 mm, and the length is 56.0 mm (b) The experimental setup of light treatment with surface MLs and distributed catalysts particles. (c) Chemical structures of photodegraded pollutants, including methyl orange (MO), norfloxacin (NFX), sulfadiazine (SFD), and sulfamethoxazole (SMX).

analyzing optical photos with Image J. The height of random MLs and high-curvature MLs array was separately characterized with atomic force microscope (AFM, Bruker, tap mode) and confocal microscope (Zeiss Axio CSM 700). A transmission mode confocal microscopy (Leica SP8) was applied to measure the focal distance of MLs in the array. An intensity profile was obtained after a vertical scanning of the ML array-decorated substrate. The focal distance was defined as the distance between the brightest point in the intensity profile and the substrate surface.

2.2. Fabrication and characterization of MLs-decorated glass vials

The surface MLs can also be immobilized on a curved surface. The inner surface of a glass vial (Fisherbrand Class A clear glass vial) with a volume of 30 mL was hydrophobized by coating OTS onto the surface. The vial with a hydrophobic inner surface was firstly filled with 12 mL of a solution (solution A) composed of 7.6 vol% MMA, 0.8 vol% photoinitiator, 45.8 vol% water, and 45.8 vol% ethanol. Then, Milli Q water saturated with MMA and photoinitiator (solution B) was dripped into the standing vial through two tubes and two syringe pumps. The ends of the tubes were set at the opening of the vial, on the left side and right side of the vial, respectively. The flow rate in each tube was fixed at 3 mL/min. To fully replace solution A, 80 mL of solution B was added to the vial. During the solvent exchange process, the excess liquid was discharged from the vial from the opening. After the solvent exchange process, the vial was sealed and set under the UV lamp for 20 min. After removing all remaining mixtures and the washing step, the PMMA MLs-decorated vial was prepared. The morphology of the MLs-decorated vial can be observed with an optical microscope. All the parameters mentioned above were optimized in our previous work. [57]

2.3. Optical simulations of surface MLs on planar substrates

The optical simulations of surface MLs on planar substrates were conducted with Zemax OpticStudio. The glass substrate decorated with MLs was set in a horizontal plane (X-Y plane). A plane wave light source was set perpendicular to the horizontal plane (along the Z axis) with an intensity of 21.64 W/cm^2. Five horizontal light-flux detectors were set at different depths in the solution below the MLs-decorated substrate to demonstrate the top-view light irradiation profiles of both MLR and MLA. A rectangular X-Z plane monitor which crossed through the center of a single ML in the array was also inserted to describe the cross-sectional irradiation profile of the ML.

2.4. Photocatalytic degradation of pollutants with surface MLs

Surface MLs were utilized in the photocatalytic degradation of common pollutants in natural water and wastewater to enhance the photodegradation efficiency (η). To evaluate the performance of random MLs and high-curvature ML array, the planar substrate with immobilized surface MLs was assembled in a homemade chamber for the light treatment of water that contained orgnic pollutants (Fig. 1(b)). The light treatment was also conducted in the PMMA MLs-decorated glass vials to evaluate the efficiency of MLs on a curved surface on a larger scale. The pollutants involved in the degradation experiments include methyl orange (MO, 85%, Sigma-Aldrich), norfloxacin (NFX, Alta aesar), sulfadiazine (SFD, 99.0–101.0%, Sigma Aldrich), and sulfamethoxazole (SMX, analytical standard, Sigma Aldrich). The aqueous solutions of these pollutants with the analyte concentration of 5 mg/L were prepared with ultra-pure water (produced by Milli-Q Direct 16), synthetic river water, or real river water as the solvent. For the solution with ultra-pure water as the solvent, the pH value was measured at around 7 with a pH meter (Accumet AE150, Fisher Scientific).

To prepare the synthetic river water, 52.19 mg $Na_2SO_4 \cdot 10H_2O$ (Sigma Aldrich), 4.08 mg $NaNO_3$ ($\geq$ 99.0%, Sigma Aldrich), 106.96 mg $CaCl_2 \cdot 10H_2O$ (Sigma Aldrich), 100.81 mg $NaHCO_3$ (certified ACS, Fisher Chemical), 101.30 mg $MgSO_4 \cdot 7H_2O$ (Fisher BioReagents), 2.56 mg humic acid (technical grade, Aldrich), and 5.32 mg alginic acid (Acros organics) were dissolved in 1 L ultra-pure water. The real river water was collected from Whitemud Creek to the North Saskatchewan River in Edmonton, Alberta, Canada at 9:30 am on April 26, 2022. Both the synthetic water and real river water were characterized by a total

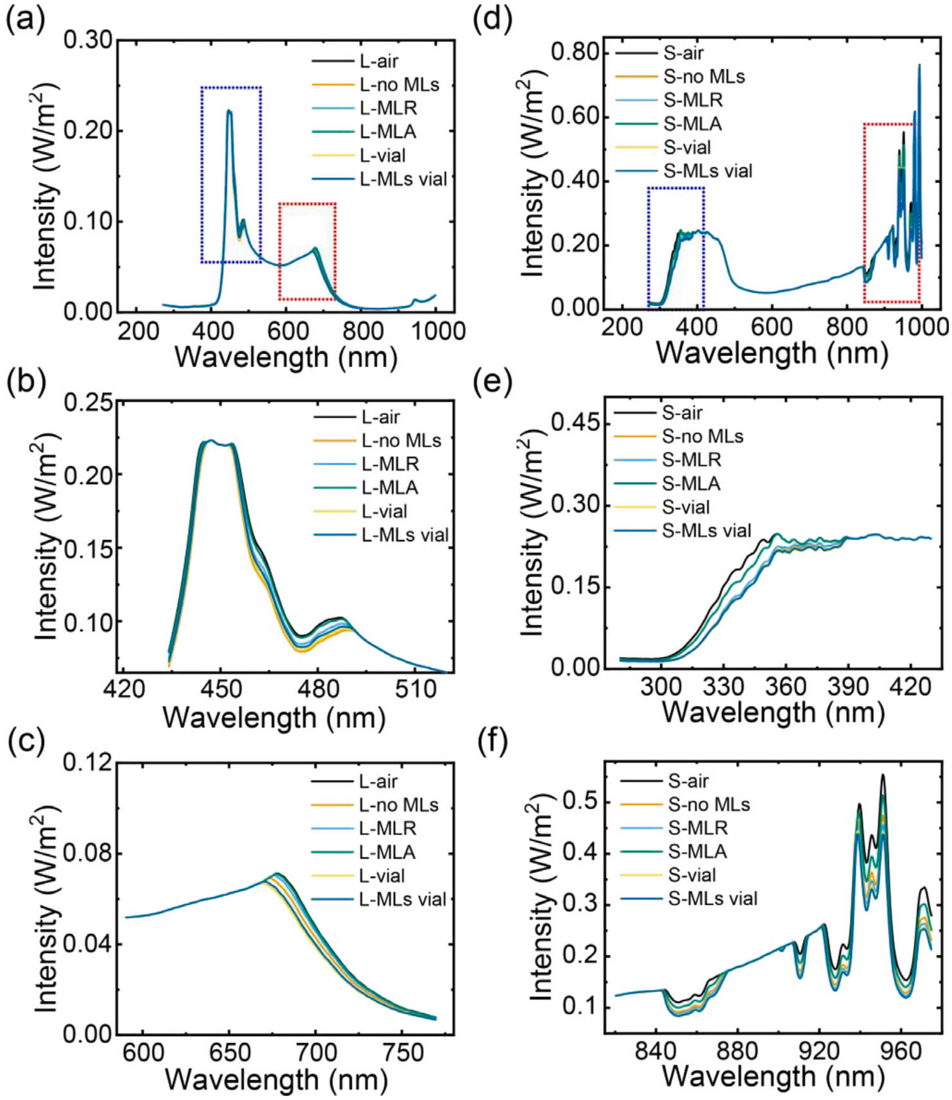

Fig. 2. Spectra of light from visible LED lamp (intensity: 21.64 W/m^2) and from simulated solar light (intensity: 1 Sun) at the position of light treatment reactor. (a) Spectra of light from the visible LED lamp after transmitting through the air or top surface of the reactor. The zoomed-in spectra are shown in (b) (from 415 to 515 nm) and (c) (from 585 to 775 nm). (d) Spectra of the light from simulated solar light after transmitting through the air or the top surface of the reactor. The zoomed-in spectra are shown in (e) (from 285 to 435 nm) and (f) (from 820 to 775 nm).

Table 1
Concentration of ions in the synthetic water (Unit: mM).

Ion type	SO_4^{2-}	Cl^-	NO_3^-	Na^+	Ca^{2+}	Mg^{2+}
Conc./mM	8.3	5.3	0.046	2.1	0.85	0.47

organic carbon (TOC) analyzer (TOC-L Series, SHIMADZU), a pH meter (Accumet AE150, Fisher Scientific), and ion chromatography (Dionex ICS-5000, Thermo Scientific). The synthetic river water had a pH value of 7.3, a TOC value of 3.8 mg/L, and a COD value of 9.2 mg/L, while the river water had a pH of 7.5, a TOC value of 25.6 mg/L, and a COD value of 163.3 mg/L. The concentrations of ions in the synthetic are displayed in Table 1. SMX and MO were spiked in the synthetic river water and the real river water for the light treatment with the same concentration of 5 mg/L.

One of the commercialized photocatalysts, zinc oxide (ZnO, certified ACS powder, Fisher Chemical), was dispersed in the aqueous solutions containing different types of pollutants by a sonication step for 20 min. All the solutions were stored in a dark environment at a temperature of 4 °C except the light treatment process. The catalyst was dispersed in the aqueous solutions with sonication in the dark environment for 30 min to ensure sufficient adsorption of the pollutant on the surface of the catalysts. To assess the performance of surface MLs with varied amounts of ZnO, multiple concentrations of ZnO dispersed in the pollutant solutions (ultra-pure water as the solvent) were used, including 5 mg/L, 10 mg/L, 50 mg/L, and 100 mg/L. In addition to ZnO, titanium dioxide (TiO_2, 21 nm primary particle size, ≥ 99.5%, Aldrich chemistry) was used to verify the efficiency of surface MLs under different types of catalysts. To compare the performance of MLs when using each type of the catalyst, the initial concentrations of TiO_2 and ZnO were set at 5 mg/L. The band gap of ZnO and TiO_2 was 3.26 eV and 3.25 eV, respectively, which were measured with diffusion reflectance spectrum (Hitachi U-3900H) and Tauc plot (shown in Supplementary information, Figure S1 (c–d)) [66].

A visible LED lamp (SOLIS-3C, Thorlabs) and a simulated solar light (SS200AAA Solar Simulation System, Photo Emission Tech) were used as light sources for the photocatalytic degradation of pollutants in water. The distance between the upper surface of the reactor and the light source was fixed at 23.5 cm for the visible light LED and 35.7 cm for the simulated solar light source. A series of irradiation conditions (shown in Table 2) were tested in this work by changing the light sources, the glass substrate, and the type of surface MLs. The spectra

Table 2
Light sources and MLs for light treatment.

Name	Light source	Substrate type	MLs type
L-air	Visible LED	/	/
L-no MLs		Planar glass substrate	/
L-MLR		Planar glass substrate	MLR
L-MLA		Planar glass substrate	MLA
L-vial		Glass vial	/
L-MLs vial		Glass vial	MLR
S-air	Simulated solar	/	/
S-no MLs		Planar glass substrate	/
S-MLR		Planar glass substrate	MLR
S-MLA		Planar glass substrate	MLA
S-vial		Glass vial	/
S-MLs vial		Glass vial	MLR

Table 3
Conditions of photodegradation of organic components.

Light source	MLs type	Catalyst	Catalyst conc. (mg/L)
Visible LED	MLR	/	/
	MLA	/	/
	/	ZnO	100/50/10/5
	MLR	ZnO	100/50/10/5
	MLA	ZnO	100/50/10/5
	/	TiO_2	5
	MLR	TiO_2	5
	MLA	TiO_2	5
Simulated solar	/	ZnO	100/10
	MLR	ZnO	100/10
	MLA	ZnO	100/10
	vial	ZnO	10
	MLs vial	ZnO	10

of the irradiation above the reactors were collected with a portable spectrometer (StellarNet Inc) at the top position of reactors, as shown in Fig. 2(a). In order to assess the influence of the irradiation conditions listed in Table 2 on the irradiation exposed to the treated solution, the spectra of light that transmitted through the top surface of the reactor (Fig. 2(b–g)) were obtained by setting the detection sensor of the spectrometer under the top surface of different reactors. The power output of the light sources was adjusted to investigate the influence of the light intensity on the MLs-enhanced photocatalytic degradation process.

All the light treatment conditions involved in this study are summarized in Table 3, and each condition is represented with the name listed in Table 2 according to the light source and MLs applied in the treatment, the type of catalysts, and the concentration of catalyst (unit: mg/L). The MLs-involved photocatalytic degradation process was studied by various analytical instruments. The degradation efficiency (η) is calculated based on Eq. (1), where C_i is the initial concentration of a pollutant after the adsorption of pollutants reached equilibrium and C_f is the final concentration of the pollutant after the light treatment. For the solution containing pollutants prepared with ultra-pure water, the concentration change of a pollutant could be identified with UV-visible spectroscopy (UV–Vis, Thermo fisher, Genesys 150). According to the Beer–Lambert Law, the absorbance (A) of an analyte in the solution is proportional to its concentration (C) if the analyte concentration is within a linear range. The relationship between absorbance and concentration is shown in (2) (ε: molar attenuation coefficient, L: light path). The concentrations of organic analytes involved in this work were within the linear range, and the evidence was included in the supporting information (Figure S1). Therefore, the η of a pollutant can be calculated by Eq. (3) by combining Eqs. (1) and (2). A_i and A_f are the absorbance at the representative peak [67] of a pollutant before and after the treatment, respectively.

$$\eta = \frac{C_i - C_f}{C_i} \times 100\% \tag{1}$$

$$A = \varepsilon C L \tag{2}$$

$$\eta = \frac{C_i - C_f}{C_i} \times 100\% = \frac{A_i - A_f}{A_i} \times 100\% \tag{3}$$

For the solution containing pollutants prepared with the synthetic water, the concentration changes of analytes were characterized by an ultra-performance liquid chromatography-mass spectrum (UPLC-MS, ACQUITY UPLC H-Class, Waters). The method to detect SMX with UPLC-MS was included in supporting information. All solutions containing photocatalyst suspends were centrifuged for 10 min at 14,000 rpm, and then only the supernatant was used for analysis.

The performance of the photocatalysts was influenced by many factors associated with the irradiation conditions (such as intensity, photon absorption, light scattering, etc.), catalyst properties, adsorption of pollutants, properties of water matrices, and chemical properties of organic contaminants. In order to show the enhancement of photocatalytic degradation efficiency obtained by implementing surface MLs, all the parameters except the usage of MLs were kept constant. The ability of surface MLs to enhance η of pollutants was quantified with an enhancement factor (f) which was defined by Eq. (4)

$$f = \frac{\eta_{(MLs+catalyst)}}{\eta_{catalyst}} \tag{4}$$

The reaction mechanisms may be further understood from the balance between the mass of CO_2 generated from the complete degradation of organic contaminants and the mass decrease in solutions containing contaminants [68,69]. However, as shown in Fig. 1(b), our reaction systems were fully sealed with negligible mass transfer from the system during the irradiation. In addition, it was almost impossible to quantify the CO_2 production from our systems due to the small volume of our samples and the dissolution of CO_2 in water. The total amount of the model contaminant in the treated solution was 10 μg. Even from complete degradation, only 17 to 22 μg CO_2 would be produced at maximum. CO_2 production from the photodegradation of organic contaminants in MLs-enhanced photocatalytic systems may be conducted in the future after modification of the experimental setup. Instead of mass balance to monitor the reaction mechanism, the characterization of free radicals generated in the photocatalytic system was feasible to reveal the degradation mechanism in the presence of surface MLs [70,71].

The presence of free radicals in the photocatalytic degradation process was verified with an electron spin resonance (ESR) spectrum (Elexsys E-500, Bruker). The ultra-pure water dispersed with ZnO (10 mg/L) was irradiated by the visible LED lamp or the simulated solar light for 30 min before the ESR detection. 5,5-Dimethyl-1-pyrroline N-oxide (DMPO, Sigma Aldrich), as a spin-trapping agent, was used to capture the hydroxyl free radicals in the treated solution. DMPO was added to the treated solution with a concentration of 5.7 g/L just before the light treatment started. The solution was added into quartz (CFQ) ESR tubes (outside diameter: 5 mm) to detect free radical signals immediately after the irradiation. The ESR spectrum of methanol dispersed with ZnO (10 mg/L) under MLA was also obtained after the irradiation by simulated solar light for 30 min (shown in supporting information, Figure S2).

3. Results and discussion

3.1. Morphology and optical properties of MLs

The redistribution of light irradiation is determined by the morphology and spatial arrangement of surface MLs. The MLs on the pre-patterned substrate (MLA) are arranged in a highly-ordered array with a uniform radius of 6.5 μm due to the confinement of hydrophobic domains, as shown in Fig. 3(b). The surface coverage rate and the contact angle of MLA are 49° and 63.7%, respectively. The light intensity

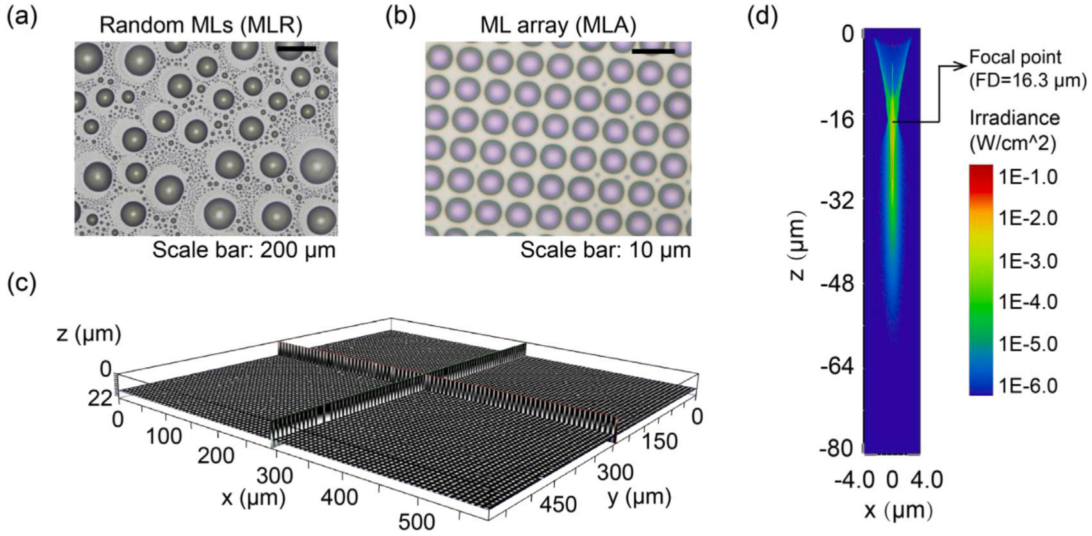

Fig. 3. Images of (a) random MLs (scale bar: 200 μm) and (b) ML array (MLA) (scale bar: 10 μm) obtained with optical microscope. (c) The light intensity profile of MLA with confocal microscope (scale bar: 100 μm). (d) The cross-sectional light intensity of a single ML in the array. The point with the highest irradiance value is the focal point. The position with $z = 0$ is the substrate surface. The focal distance is the distance between the focal point and the substrate surface.

profiles of MLA obtained from the confocal microscope and optical simulation results of a single ML from the ML array are displayed in Fig. 3(c) and (d), respectively. Due to the uniform size, the focal distances of MLs in the array have the same value. From the light intensity profiles, it is found that the focal points of MLA are located in a horizontal plane which is around 16 μm away from the substrate. As a comparison, the focal distance of a single ML in the array is 16.5 μm according to the optical simulations. Therefore, the simulated focal distance is consistent with that obtained from the confocal microscope.

Another type of surface MLs, represented with MLR, is fabricated on homogeneous substrates. MLR are randomly distributed on the planar substrate, and their diameters vary from 2 μm to 200 μm with a fixed contact angle of 7.5°. The surface coverage rate of MLR is 47.2%. The focal distances of MLR differ due to the existence of the size distribution among them. Therefore, it is difficult to measure the focal distances of MLR with a confocal microscope.

The top view intensity profiles of surface MLs in Fig. 4(a–b) exhibit the distribution of irradiance at the horizontal plane with certain depths. At the horizontal plane at certain depth, the spot that has the maximum incident flux value is considered as the spot with the highest intensity at this depth. As the depth changes, the maximum incident flux value also fluctuates. At the depth of 16.5 μm which is close to the focal distance of MLA, the maximum incident flux value under MLA is the highest, reaching 2.95×10^{-8} W. The number of the spots with the highest value is 400 on the horizontal plane with an area of 2.25×10^{-2} mm^2. In comparison, the highest maximum incident flux value under MLR is 2.26×10^{-7} W located at the depth of 225.5 μm. However, only two spots reach 2.26×10^{-7} on the horizontal plane under random MLs within the same area. Therefore, the maximum total incident flux over the horizontal plane of MLA is around 26 times larger than that of MLR.

When the depth increases, the maximum incident flux value under MLA significantly drops, while the value under MLR first increases and then gradually diminishes. As the depth changes from 16.5 μm to 797.5 μm, the maximum flux value under MLA decreases by 56%, while the value under MLR increases by 3.6 times. The variation of focal distances of MLR avoids the sharp decay of irradiation intensity along the Z direction but also causes a lower maximum total incident flux value. In summary, the uniformity of focal distances of MLA can reach a maximum flux, higher than MLR, but the decay irradiation intensity along the Z axis is much more rapid.

3.2. Free radicals in the presence of MLs

The reflectance specta of ZnO and TiO_2 powders (Fig. 5(a)) and the absorbance spectra of ZnO suspension with different concentrations (Fig. 5(b)) indicate that the catalysts applied in the light treatment partially absorb visible light under the irradiation of visible LED and simulated solar light. The existence of free radicals is verified by the electron spinning resonance (ESR) spectra. Based on the spectra obtained by ESR (Fig. 5(c)), no obvious signals can be observed when neither ZnO nor surface MLs are used in the light treatment. Under both visible LED light and simulated solar light, a similar curve shape is observed when ZnO is added to the system. As described in the literature [70], the spectra indicate that ·OH free radicals form after ZnO particles absorb the energy from either visible LED or simulated solar light. The formation of ·OH accelerates the degradation of pollutants. When MLA is applied together with ZnO, the signals of free radicals become stronger under both visible LED light and simulated solar light. Therefore, it is possible that more free radicals are generated by utilizing MLA. Consequently, more free radicals bring about the higher degradation efficiency (η) [72].

Stronger signals of free radicals observed in the system with MLA could be attributed to the higher light intensity at the focal points of MLs. Based on the second law of photochemistry, [73,74] higher light intensity leads to a higher concentration of reactive species, such as hydroxyl free radicals in the MLs-enhanced photocatalytic system [75,76]. The light intensity at focal points of surface MLs increases by several times as shown by the optical simulation results (Fig. 4). A higher concentration of active species in the MLs-induced system is confirmed by ESR characterization in our previous work. [57]. Similar to the photolysis system without catalysis, the ESR spectra in Fig. 5 suggest that the photodegradation with ZnO as the catalyst can also be accelerated, due to the larger amount of free radicals from the focusing effect of surface MLs.

The increase in the concentration of free radicals is the consequence of the stronger local irradiance intensity in the presence of surface MLs. However, the types of free radicals are not expected different from the situation without MLs, as the types are only determined by the light source and the type of photocatalyst. TiO_2 used in our experiments is

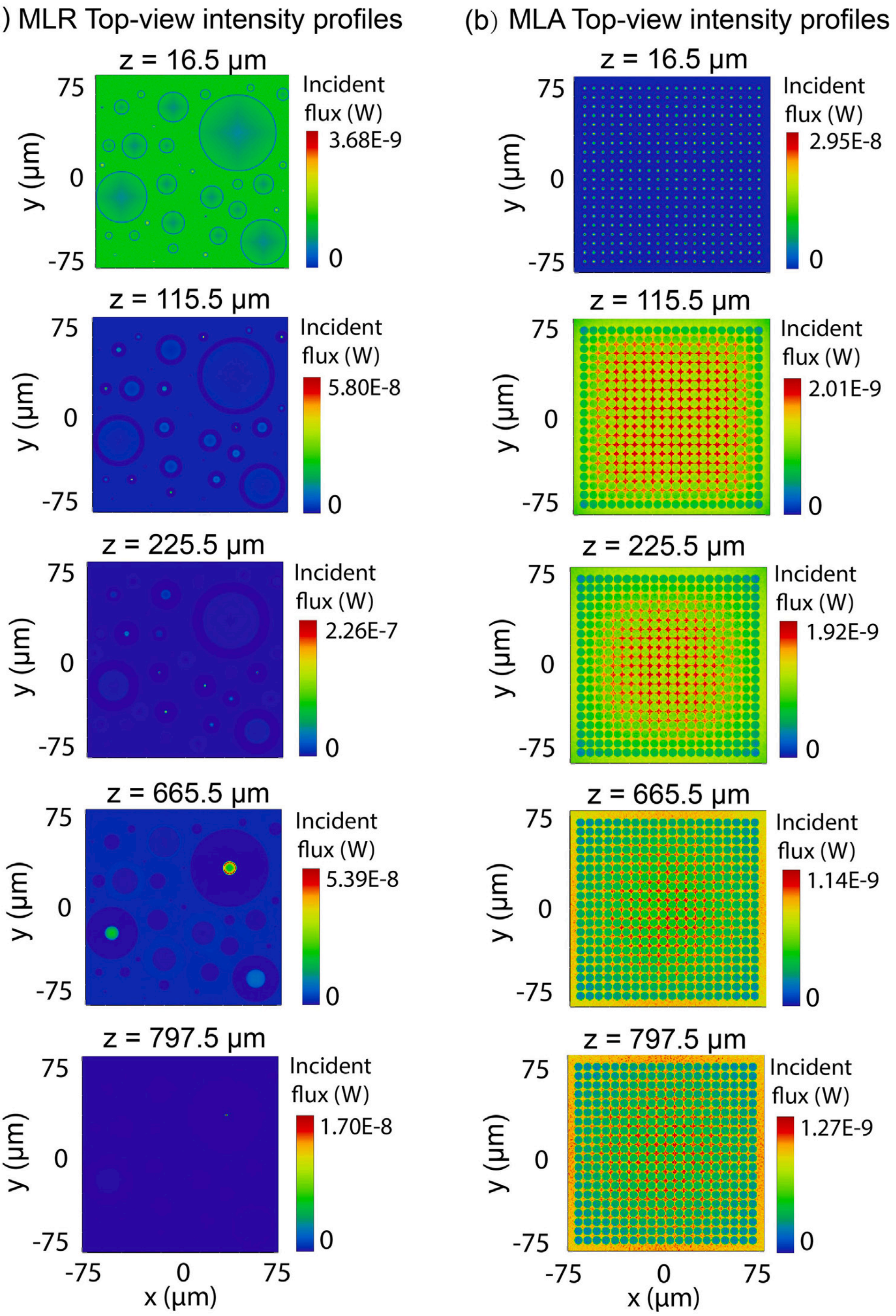

Fig. 4. Top view intensity profile under (a) MLR and (b) MLA at the horizontal plane with the distance of 16.5 µm, 115.5 µm, 225.5 µm, 665.5 µm, and 797.5 µm away from the substrate surface.

a commercialized photocatalyst that has been widely studied [77,78]. According to ESR results reported in the literature, we could conclude that hydroxyl free radicals form when TiO_2 acts as the photocatalyst, which promotes the degradation of organic pollutants.

3.3. *Influence of catalyst concentration on the efficiency of photocatalytic degradation under visible light*

The absorbance curves of the solutions containing different pollutants before and after light treatment are plotted in Fig. 6. For the four pollutants treated under a visible LED lamp, slight enhancement can be observed by only applying surface MLs. By comparing the two types of surface MLs, MLA performs better than MLR since the decrease of absorbance peak is more obvious.

As shown in the second column of the plots in Fig. 6, the reduction in absorbance values of all pollutants in the presence of ZnO particles improves. Such improvement becomes larger when we increase the initial concentration of ZnO. By combining surface MLs with ZnO particles, the absorbance peaks of pollutants further become smaller. In the presence of ZnO, more reduction of absorbance value is also observed with MLA compared with MLR, indicating the higher removal rates of pollutants with MLA.

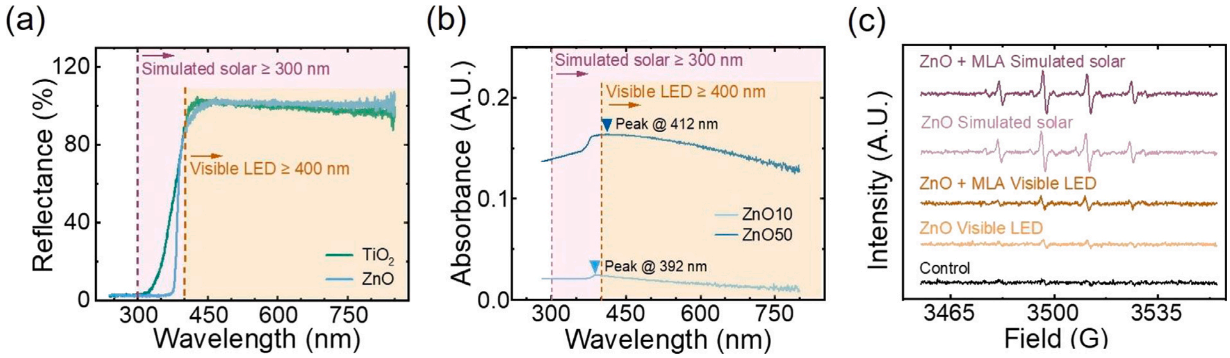

Fig. 5. (a) Reflectance spectra for ZnO and TiO$_2$ particles with diffusion reflectance spectroscopy. (b) UV–Vis absorbance spectra of ZnO suspension in Milli Q water with the concentration of 10 mg/L and 50 mg/L. The minimum wavelength of the visible LED and simulated solar light is 400 nm and 300 nm, respectively. (c) Electron spinning resonance (ESR) spectra under different conditions after light treatment of 30 min. (The black curve is for the condition without ZnO particles and surface MLs. The light blue curve represents the treatment with only ZnO particles, while the dark blue curve is for both ZnO and MLA under a visible LED lamp. The light orange curve is for the conditions with only ZnO particles, while the dark orange curve is for both ZnO and MLA under simulated solar light.)

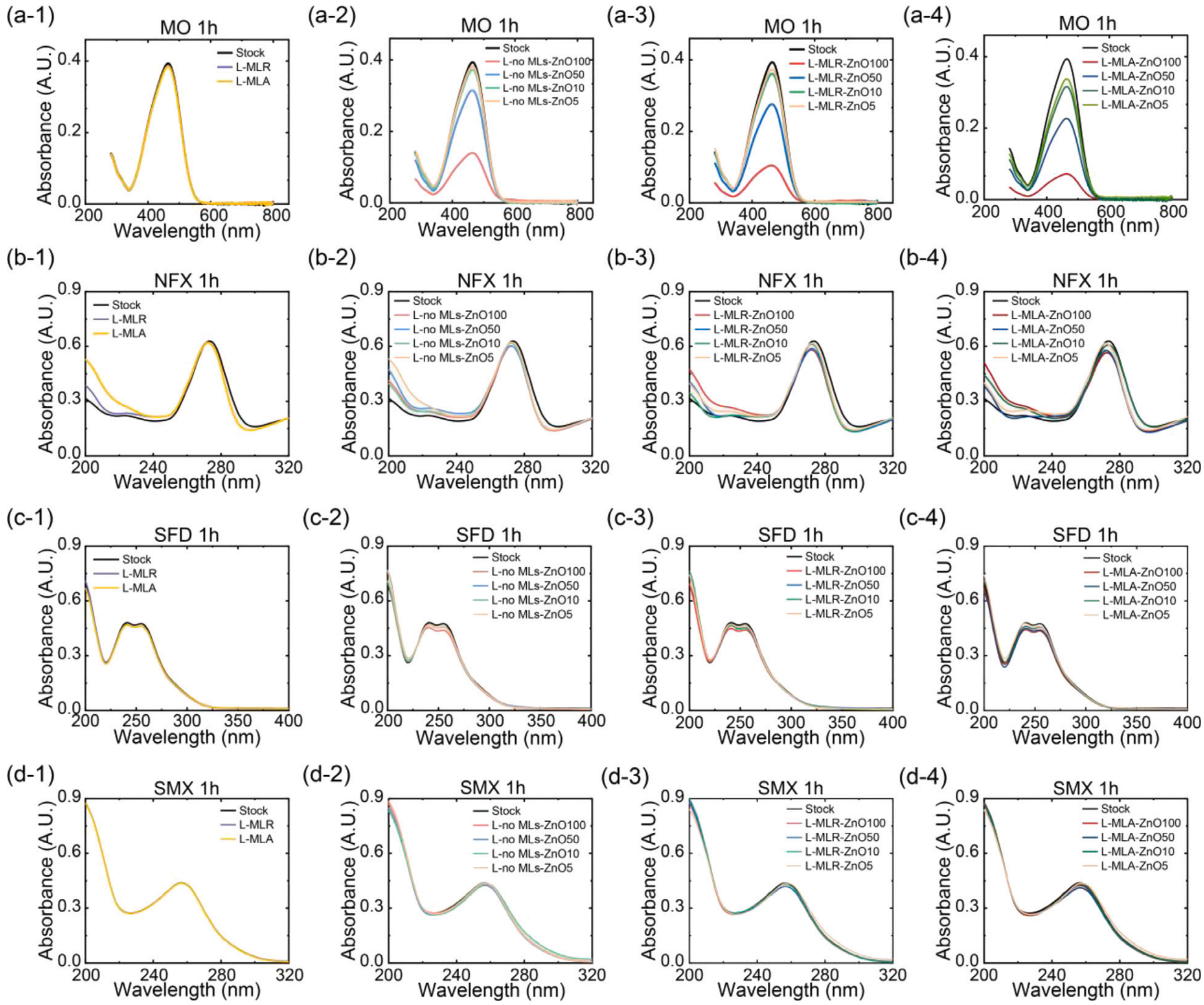

Fig. 6. Representative absorbance spectra of pollutants (MO in (a–1) to (a–4), NFX in (b–1) to (b–4), SFD in (c–1) to (c–4), and SMX in (d–1) to (d–4)) with surface MLs and ZnO (under visible LED) after light treatment with 1 h.

The photodegradation efficiency of all pollutants under the visible LED light is plotted over the concentration of ZnO in Fig. 7(a). As the concentration of ZnO particles increases, η of all four pollutants is enhanced. However, the enhancement of η by adding dispersed ZnO particles into the solutions differs with the type of pollutants. For the photodegradation of MO with ZnO, η after the irradiation of 1 h is improved by 59.2% when the ZnO concentration increases from 5 mg/L to 100 mg/L. For the other three pollutants, the change of η after enhancing ZnO concentration from 5 mg/L to 100 mg/L is much smaller than that of MO, which is 5.7% for NFX, 2.9% for SFD, and

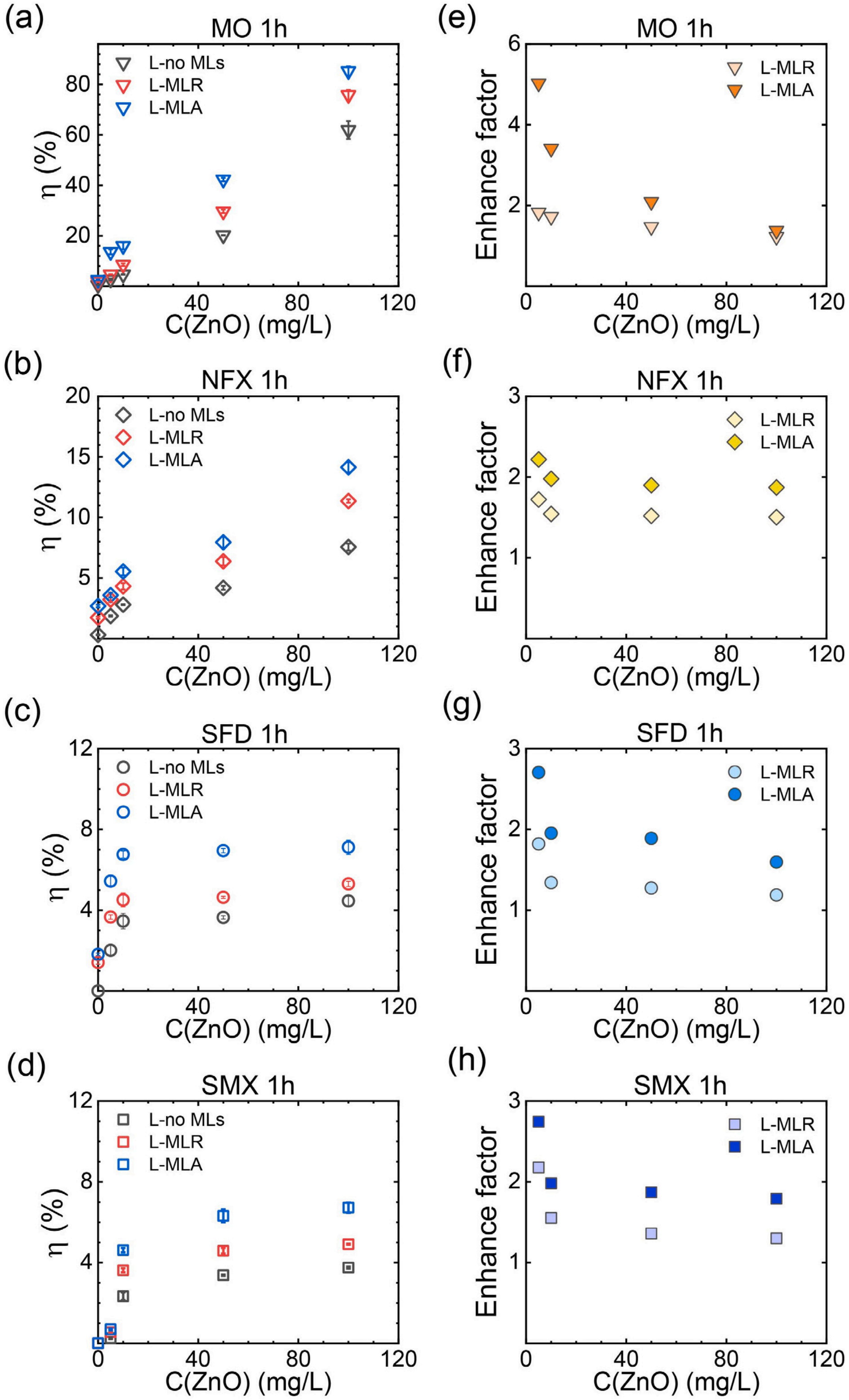

Fig. 7. Photodegradation efficiency of (a) MO, (b) NFX, (c) SFD, (d) SMX using surface MLs and ZnO with different concentration (under visible LED). Enhancement of photodegradation efficiency of (e) MO, (f) NFX, (g) SFD, (h) SMX by using surface MLs.

2.3% for SMX. The pollutant that is more difficult to degrade, which is SMX, has the least improvement when increasing the concentration of ZnO. The different degradation mechanisms among the pollutants may lead to the varied effectiveness of ZnO. Much higher *η* efficiency of MO degradation is possibly related to the sensitization mechanism for azo dyes. Charges are produced as the MO molecules are excited under irradiance and then injected in photocatalysts and oxidized dye for subsequent degradation [79,80]. In contrast, the sensitization mechanism does not apply to other tree organic compounds, including NFX, SFD, and SMX, since they are transparent to the irradiation wavelengths. Regardless of the details in photodegradation mechanisms for those

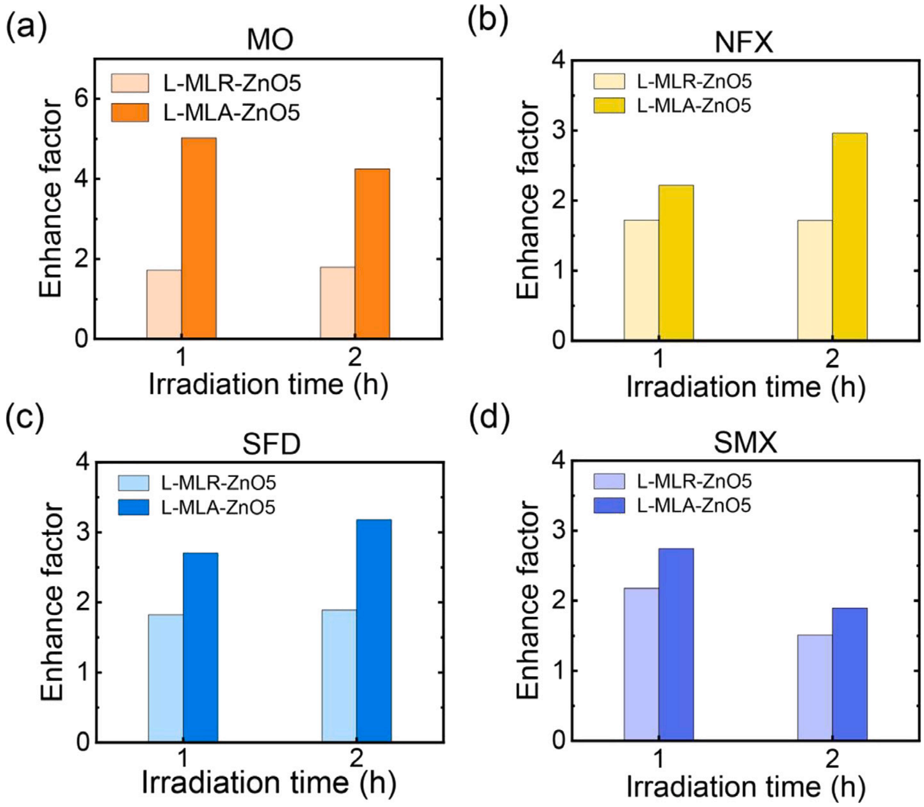

Fig. 8. Enhancement factor of ZnO-photocatalyzed degradation efficiency of (a) MO, (b) NFX, (c) SFD, (d) SMX with surface MLs after irradiation time of 1 h and 2 h.

organic contaminants, the enhancement in η is achieved for all of them by adding ZnO.

Comparing with the situation only implementing ZnO or only surface MLs, the treatment with both MLs and ZnO achieves higher η, indicating the synergistic effect in the surface MLs-enhanced photocatalytic system. By applying surface MLs in the photocatalytic degradation process with ZnO as the catalyst, the distinguished enhancement of η can be confirmed in all four pollutants. The variance in the enhancement of η is resulted not only from using surface MLs but also from the increase in ZnO concentration, which is similar to the situation only adding ZnO in the reaction systems. The photocatalytic degradation exhibited higher η with MLA compared with that using MLR. The possible reason for the more outstanding effect of MLA is the more efficient irradiation redistribution based on the highly-ordered structure in MLA, which is also demonstrated in the optical simulations [81].

The enhancement factor for the MLs-enhanced photodegradation using ZnO as the catalyst is calculated with Eq. (4). As shown in Fig. 7(e–h), the enhancement factor becomes lower at higher ZnO concentrations. The amount of active species is the key factor determining the rate of photodegradation. In the photodegradation enhanced by ZnO and surface MLs, the number of active species is up to the dosage of ZnO and the number of hot spots created by MLs [42,82]. The total number of active species (N_{total}) can be estimated using Eq. (5). In the equation, $N_{catalyst}$ is the number of active species generated due to the excitation of ZnO, and N_{MLs} is the number of active species attributed to the focus effect of MLs. The photocatalytic degradation efficiency is dependent on the number of active species in the system. Therefore, the enhancement factor with MLs is positively related to the ratio of N_{MLs} and $N_{catalyst}$ in Eq. (6). With an increase in the concentration of ZnO, $N_{catalyst}$ also increases while N_{MLs} is fixed, therefore, the enhancement factor drops down.

$$N_{total} = N_{catalyst} + N_{MLs} \tag{5}$$

$$f \sim \frac{N_{total}}{N_{catalyst}} = 1 + \frac{N_{MLs}}{N_{catalyst}} \tag{6}$$

The enhancement factor in η of ZnO-photocatalytic degradation by surface MLs is also monitored with the elongated irradiation time of light treatment. The enhancement factor for the four organic pollutants is plotted with the irradiation time in Fig. 8. For MO and SMX, the factor becomes smaller when the irradiation time increases from 1 h to 2 h. Reversely, the factor grows in the photocatalytic degradation of NFX and SFD during a longer treatment time. The difference in the enhancement factor not only is due to the type of pollutants but is also related to the properties of MLs. The enhancement factor obtained by MLR shows less change than that by MLA after the longer irradiation time.

3.4. General enhancement of photocatalytic degradation with surface MLs under visible light

The effectiveness of surface MLs is verified by using a different catalyst in the photocatalytic degradation process. As shown in Fig. 9(a–d), more decrease in absorbance peaks is presented when TiO_2 is used as the catalyst compared to that without a catalyst. When combining TiO_2 with surface MLs, more organic pollutants are degraded than those in the treatment with only TiO_2. After the same light treatment process, the MLA-enhanced photocatalytic degradation with TiO_2 has the most decrease in absorbance peak values.

The η values of all pollutants after the irradiation of 1 h with only TiO_2 or with both TiO_2 and MLs are displayed in Fig. 9(e). The η values of all four pollutants have been further improved after applying MLs in the photocatalytic degradation with TiO_2. Moreover, MLA shows more enhancement compared to MLR. The enhancement factor by using MLR and MLA are shown in Fig. 9(f). The effect of surface MLs on the degradation catalyzed by TiO_2 is similar to that catalyzed by ZnO. Therefore, surface MLs accelerate photocatalytic degradation, regardless of the types of catalysts.

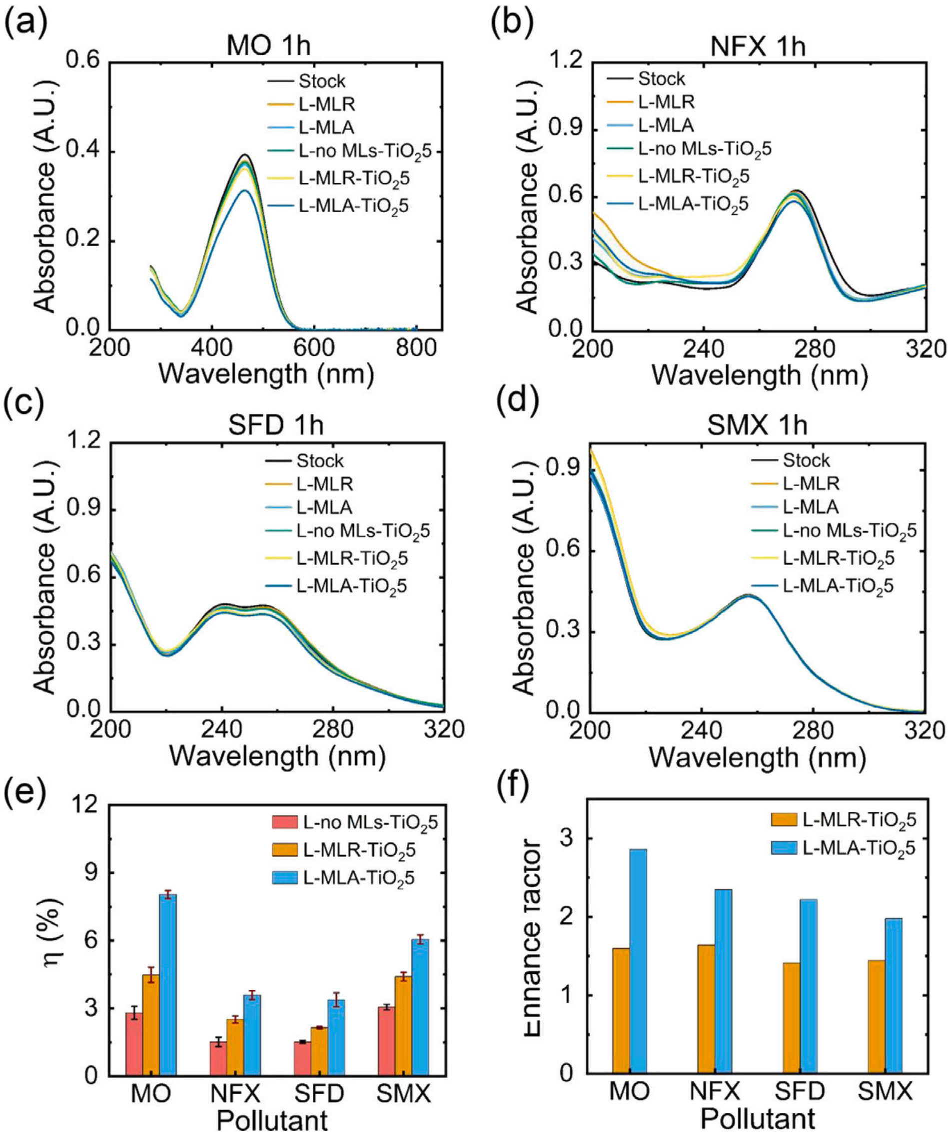

Fig. 9. Representative absorbance curves of (a) MO, (b) NFX, (c) SFD, (d) SMX after the light treatment under the visible LED lamp for 1 h. (e) Photodegradation efficiency and (f) enhancement factor of TiO_2-photocatalytic degradation efficiency of pollutants with surface MLs after irradiation time of 1 h.

3.5. MLs-enhanced photocatalytic degradation under simulated solar light

The representative absorbance spectra of SMX solution after the irradiation under different conditions are shown in Fig. 10(a–d). By comparing Fig. 10(a) and (c), it is found that the absorbance peak drops faster when the concentration of ZnO increases. As shown in Fig. 10(a) and (b), the decrease of absorbance peak value is higher when MLA is used in the light treatment. Such difference is also displayed in Fig. 10(c) and (d), where the concentration of ZnO changes to 10 mg/L.

The η values of all conditions presented in Fig. 10(a–d) are plotted in Fig. 10(e). For the concentration of ZnO equal to 100 mg/L, η reaches 72.4% within 3 h when both MLA and ZnO were used. To achieve a similar η with the ZnO concentration of 10 mg/L, around 5 h is required in the presence of MLA. The η under the simulated solar light is higher than that under the visible LED light due to the difference in light intensity and the wavelength range of irradiation.

The degradation efficiency of SMX with MLA is higher than that without MLA under the simulated solar light, which is the same phenomenon under visible light. The enhancement factors by MLA with two concentrations of ZnO under the simulated solar light are plotted with the irradiation time in Fig. 10(f). When the concentration of ZnO is 100 mg/L, the enhancement factor fluctuates around 1.2 as the irradiation time changes from 1 h to 3 h. For the photocatalytic degradation with a ZnO concentration of 10 mg/L, the enhancement factor by MLA is higher than that with 100 mg/L of ZnO. However, the factor drops from 1.6 to 1.4 as the irradiation time increases from 1 h to 8 h. The results under the simulated solar light reveal that the ordered spatial arrangement of MLs is optimal for photocatalytic degradation when the light source is closer to real solar light. The higher enhancement factor under the lower concentration of ZnO further validates our assumption shown in Eq. (6) under simulated solar light.

The η of MLs-enhanced photocatalytic degradation of SMX is positively correlated with the intensity of simulated solar light in the range from 0.3 Sun to 1 Sun (Fig. 11(a–b)). As the irradiation time increases from 1 h to 2 h, the enhancement of η by improving the intensity of light is different. As the light intensity increases from 0.3 Sun to 1 Sun, the η increases from 2.1% to 5.6% only using ZnO during the irradiation of 1 h, while the η is enhanced from 4.3% to 9.0% by using ZnO combined with MLA during the same irradiation time. (Fig. 11(a)) The enhancement in η becomes larger when the irradiation time increases to 2 h based on Fig. 11(b).

In addition, the η of SMX with both of MLA and ZnO is always higher than that with only ZnO under varying light intensities. The

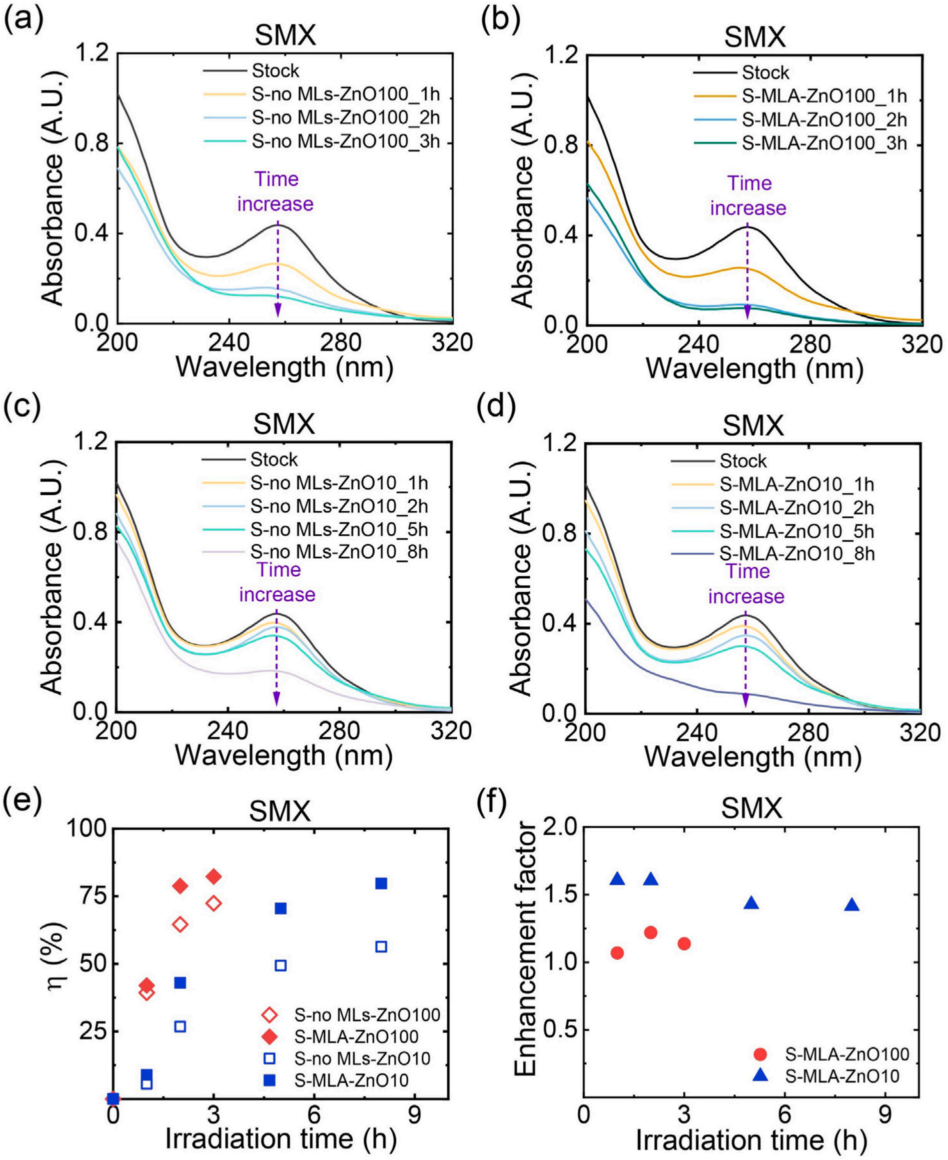

Fig. 10. Representative absorbance curve of SMX solution after the light treatment with (a) only ZnO particles with a concentration of 100 mg/L (b) both ZnO with a concentration of 100 mg/L and MLA (c) only ZnO particles with a concentration of 10 mg/L (d) both ZnO with a concentration of 10 mg/L and MLA under the simulated solar light. (e) Photodegradation efficiency and (f) enhancement factor of SMX under different conditions.

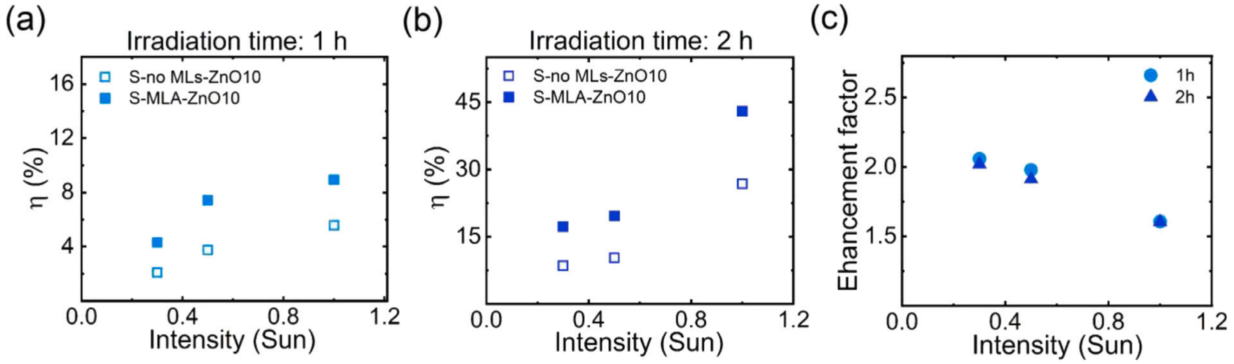

Fig. 11. Photodegradation efficiency of SMX after the irradiation for (a) 1 h and (b) 2 h under the irradiation of the simulated solar light with different intensities. (c) The enhancement factor of η by using MLA during the irradiation for 1 h and 2 h.

enhancement factor obtained by using MLA is shown in Fig. 11(c). Under irradiation with the same light intensity, the change of the enhancement factor after adding the irradiation time from 1 h to 2 h is less than 0.6. The influence of irradiation duration on the performance

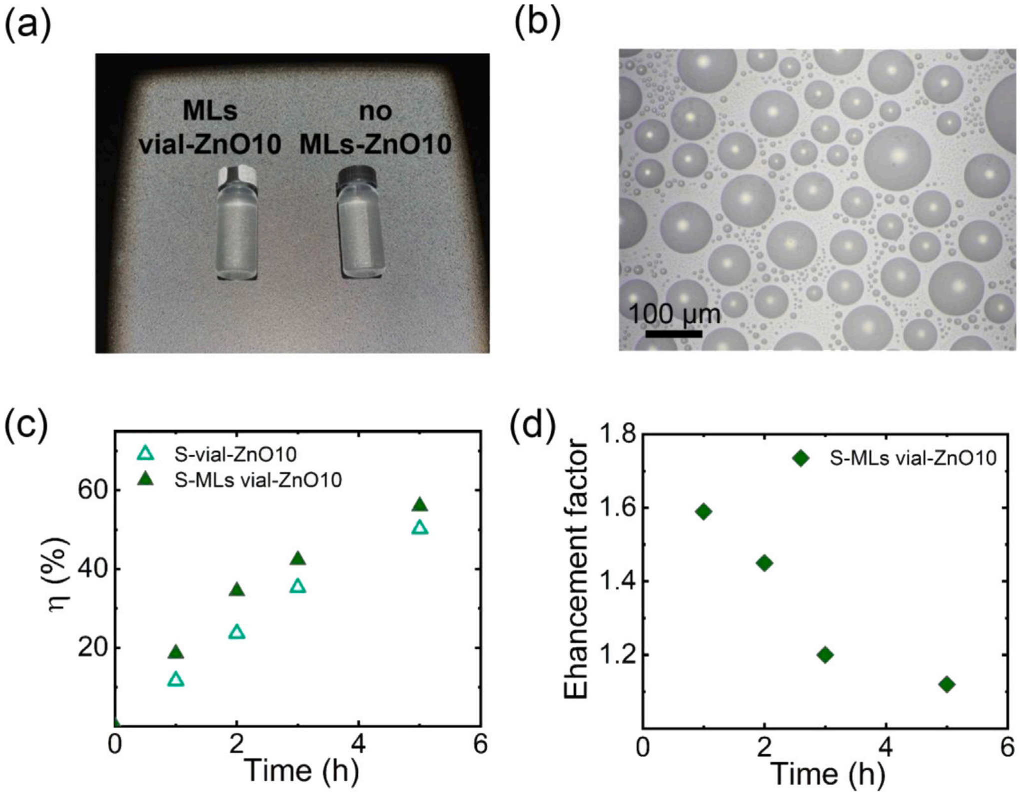

Fig. 12. (a) Experimental set-up of ZnO-photocatalyzed degradation of SMX solution with the MLs-decorated vial (C(ZnO)=10 mg/L, C(SMX)=5mg/L, pH=7.0). (b) The optical image of the MLs on the inner wall of a glass vial. (c) Photodegradation efficiency of SMX with ZnO in a bare glass vial and an MLs-decorated vial. (d) Enhancement factor of ZnO-photocatalytic degradation with the MLs-decorated vial.

of MLA is negligible in the first two hours of photodegradation of SMX. The enhancement factor drops down when the intensity becomes higher, showing that surface MLs perform better in enhancing the photocatalytic degradation of SMX under the weaker irradiation.

3.6. MLs-enhanced photocatalytic degradation in a glass container

The MLs-enhanced photocatalytic degradation can be conducted in the MLs-decorated glass vials. As demonstrated in Fig. 12(a), the glass vial keeps transparent with surface MLs immobilized on the inner wall. In the microscopic image (Fig. 12(b)), surface MLs on the vial have various sizes and random spatial distributions because of the homogeneous hydrophobic coating on the inner surface of the vial. The diameter of MLs displayed in the picture varies from 1.40 μm to 310 μm. The surface coverage rate of the MLs is around 50%.

The application of MLs-decorated vials can also enhance the η of degradation. As shown in Fig. 12(c), the η of degradation with MLA obtained from UV–Vis spectra (supporting information, Figure S3) is always higher than that using only ZnO. Under the irradiation of simulated solar light (1 Sun), the η of SMX with ZnO (10 mg/L) reaches 50.2% after five hours of light treatment, while the value is further improved to 56.0% after using the MLs-decorated vial. As demonstrated in Fig. 12(d), the enhancement factor by using MLs-decorated vials is 1.60 after the irradiation for 1 h and then continuously decreases with the irradiation time.

The degradation of SMX is significantly influenced by the concentration of SMX. When the concentration of SMX is less than 5 mg/L, a lower concentration of SMX results in a lower degradation rate [83]. The higher degradation rate with the existence of surface MLs directly leads to a lower concentration of SMX after irradiation. Therefore, the degradation rate of SMX with surface MLs drops faster than the process happening in the bare vial. As a consequence, the enhancement factor with MLs-decorated vials decreases with time.

3.7. Effect of water matrix on MLs-enhanced photodegradation

The photocatalytic degradation of SMX with ZnO can be enhanced with surface MLs not only in ultra-pure water but also in synthetic river water and real river water. The photo in Fig. 13(a) displays the collection point of the river water. By comparing the transmittance curves of different water matrices (Fig. 13(b)), we find that the transparency of synthetic water and river water is less than that of river water, especially in the wavelength ranging from 200 nm to 500 nm.

As displayed in Fig. 13(c), the η of SMX using both MLR and MLA in the light treatment is improved compared with that only using ZnO. Similar to the results observed in ultrapure water, MLA has better performance than MLR in accelerating the photocatalytic degradation of SMX. The η by applying the same type of MLs in the photocatalytic degradation of SMX in the synthetic water is lower than that achieved in the ultra-pure water after the same irradiation duration (Fig. 10(e)). HOwever, compared with the enhancement factor by surface MLs in ultra-pure water during the same treatment time, the enhancement factor in synthetic river water is higher. For example, the enhancement factor of MLR is 1.6 and 1.4 after 2 h and 5 h of irradiation, respectively. When using MLA, the factor is 3.0 for 2 h and 2.5 for 5 h (Fig. 13(d)).

The enhancement of photocatalytic degradation is also observed when using real river water as the matrix. The photodegradation efficiency of MO in river water and the enhancement factor of η over the irradiation time are plotted in Fig. 13(e) and (f), respectively. Without utilizing ZnO, around 14% enhancement is achieved by MLA after 5 h of irradiation. Compared with the condition without the catalyst and surface MLs (control group), the degradation efficiency of MO is enhanced by a maximum of 163% with only ZnO after 5 h of irradiation. By setting MLA on the top of the light treatment chamber, the photocatalytic η of MO is further improved under the same irradiation

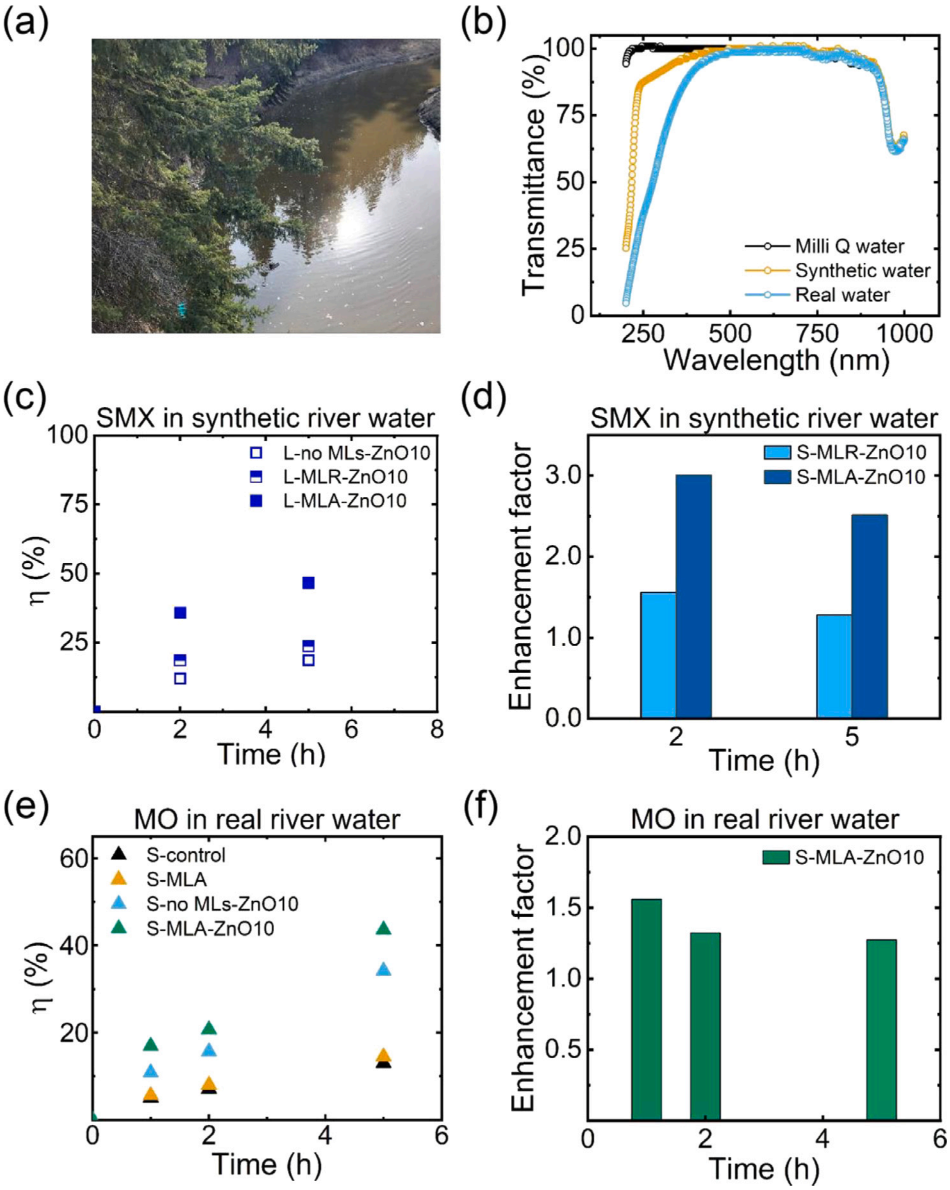

Fig. 13. (a) A photo of the real river water collection site. (b) Transmittance curves of three types of water matrices. (c) Photodegradation efficiency of SMX in simulated water under simulated solar light. (d) Enhancement factor of photocatalytic photodegradation efficiency of SMX achieved by MLR and MLA during 2 h and 5 h of irradiation. (e) Photodegradation efficiency of MO in the real river water under simulated solar light. (f) Enhancement factor of photocatalytic photodegradation efficiency of MO obtained by MLA during 1 h, 2 h, and 5 h of irradiation.

condition, which is 235% higher than the control group and 27% higher than the group only with catalyst.

The difference in η and the enhancement factor after changing the water matrix into synthetic river water or real river water can be attributed to the variation in the transmittance of water. The transmittance of the synthetic river water in the range between 200 nm and 500 nm drops as displayed in Fig. 13(b), while the decrease in transmittance of river water is even more significant. The decrease in the transmittance of the matrix is possibly caused by the light absorption from impurities in synthetic river water and real river water. As a consequence, the irradiation intensity in synthetic river water and river water should be lower than that in ultra-pure water, thus the enhancement of η by surface MLs is higher (as displayed in Fig. 11(c)).

4. Conclusions

In summary, our work demonstrates the microlenses(MLs)-enhanced photocatalytic degradation efficiency of micropollutants in water. More free radicals generated in the presence of surface MLs contribute to higher degradation efficiency. The enhancement is generally observed for all four targeted organic contaminants by using two kinds of photocatalysts. The microlens array is more effective than random microlenses in the photodegradation of all involved pollutants, which is attributed to the more effective redistribution of the irradiation energy. The performance of surface MLs, represented by an enhancement factor, varies with pollutants because of the difference in degradation mechanisms. Additionally, the enhancement in the η of photocatalytic degradation is higher at a lower concentration of the photocatalyst or under irradiation with lower intensity. Therefore, the results suggest that surface MLs have the potential for applications where the excitation of photocatalysts is suppressed due to insufficient irradiation conditions. The feasibility of surface MLs in improving decontamination is also verified in synthetic river water and a real river water matrix. In the next stage, surface MLs may be tested in the light treatment of water samples containing multiple contaminants.

Declaration of competing interest

The authors declare that they have no known competing financial interests or personal relationships that could have appeared to influence the work reported in this paper.

Data availability

Data will be made available on request.

Acknowledgments

The authors acknowledge the support from Canada First Research Excellence Fund as part of the University of Alberta's Future Energy System research initiative and the technical assistance from the Institute for Oil Sands Innovation (IOSI) at the University of Alberta. This research was undertaken, in part, thanks to funding from the Canada Research Chairs Program and Canada Foundation for Innovation. This work was also supported by a Natural Sciences and Engineering Research Council of Canada (NSERC) Senior Industrial Research Chair (IRC) in Oil Sands Tailings Water Treatment through the support of Canada's Oil Sands Innovation Alliance (COSIA), Syncrude Canada Ltd., Suncor Energy Inc., Canadian Natural Resources Ltd., Imperial Oil Resources, Teck Resources Limited, EPCOR Water Services, Alberta Innovates, and Alberta Environment and Parks. XHZ and MGED appreciates funding from NSERC Discovery Grant programs.

Appendix A. Supplementary data

Supplementary material related to this article can be found online at https://doi.org/10.1016/j.cej.2023.142345.

References

[1] D.R. Arnold, N. Baird, J.R. Bolton, Photochemistry: An Introduction, Academic Press, 2014.

[2] F. Li, J. Zhuang, G. Jiang, H. Tang, A. Xia, L. Jiang, Y. Song, Y. Li, D. Zhu, A rewritable optical data storage material system by [2 + 2] photocycloreversion-photocycloaddition, Chem. Mater. 20 (4) (2008) 1194–1196.

[3] N.-Y. Li, J.-M. Chen, X.-Y. Tang, G.-P. Zhang, D. Liu, Reversible single-crystal-to-single-crystal conversion of a photoreactive coordination network for rewritable optical memory storage, Chem. Commun. 56 (13) (2020) 1984–1987.

[4] N.R. Pradhan, J. Ludwig, Z. Lu, D. Rhodes, M.M. Bishop, K. Thirunavukkuarasu, S.A. McGill, D. Smirnov, L. Balicas, High photoresponsivity and short photoresponse times in few-layered WSe2 transistors, ACS Appl. Mater. Interfaces 7 (22) (2015) 12080–12088.

[5] A. Kimoto, J.-S. Cho, K. Ito, D. Aoki, T. Miyake, K. Yamamoto, Novel hole-transport material for efficient polymer light-emitting diodes by photoreaction, Macromol. Rapid Commun. 26 (8) (2005) 597–601.

[6] Y. Zhou, H.-Y. Zhang, Z.-Y. Zhang, Y. Liu, Tunable luminescent lanthanide supramolecular assembly based on photoreaction of anthracene, J. Am. Chem. Soc. 139 (21) (2017) 7168–7171.

[7] N. Corrigan, J. Yeow, P. Judzewitsch, J. Xu, C. Boyer, Seeing the light: advancing materials chemistry through photopolymerization, Angew. Chem. Int. Ed. 58 (16) (2019) 5170–5189.

[8] A. Bagheri, J. Jin, Photopolymerization in 3D printing, ACS Appl. Polym. Mater. 1 (4) (2019) 593–611.

[9] A. Kumar, M. Khan, J. He, I.M. Lo, Recent developments and challenges in practical application of visible–light–driven TiO_2–based heterojunctions for PPCP degradation: a critical review, Water Res. 170 (2020) 115356.

[10] Z. Luo, L. Meng, Z.T. How, P. Chelme-Ayala, L. Yang, C. Benally, M.G. El-Din, Treatment of oil sands process water by the ferric citrate under visible light irradiation, Chem. Eng. J. 429 (2022) 132419.

[11] J. Edzwald, A.W.W. Association, et al., Water Quality & Treatment: A Handbook on Drinking Water, McGraw-Hill Education, 2011.

[12] B. Sommer, A. Marino, Y. Solarte, M. Salas, C. Dierolf, C. Valiente, D. Mora, R. Rechsteiner, P. Setter, W. Wirojanagud, et al., SODIS- an emerging water treatment process, Aqua(Oxford) 46 (3) (1997) 127–137.

[13] S. Dejung, I. Fuentes, G. Almanza, R. Jarro, L. Navarro, G. Arias, E. Urquieta, A. Torrico, W. Fenandez, M. Iriarte, et al., Effect of solar water disinfection (SODIS) on model microorganisms under improved and field SODIS conditions, J. Water Suppl.: Res. Technol.—AQUA 56 (4) (2007) 245–256.

[14] M.P. Callao, M.S. Larrechi, Simultaneous determination of organic dyes using second-order data, in: Data Handling in Science and Technology, Vol. 29, Elsevier, 2015, pp. 399–426.

[15] M.A. Suara, S.O. Ganiyu, S. Paul, J.L. Stafford, M.G. El-Din, Solar-activated zinc oxide photocatalytic treatment of real oil sands process water: Effect of treatment parameters on naphthenic acids, polyaromatic hydrocarbons and acute toxicity removal, Sci. Total Environ. 819 (2022) 153029.

[16] D. Chen, Y. Cheng, N. Zhou, P. Chen, Y. Wang, K. Li, S. Huo, P. Cheng, P. Peng, R. Zhang, et al., Photocatalytic degradation of organic pollutants using TiO_2-based photocatalysts: A review, J. Clean. Prod. 268 (2020) 121725.

[17] D.S. Bhatkhande, V.G. Pangarkar, A.A.C.M. Beenackers, Photocatalytic degradation for environmental applications–a review, J. Chem. Technol. Biotechnol.: Int. Res. Process Environ. Clean Technol. 77 (1) (2002) 102–116.

[18] H. Dong, G. Zeng, L. Tang, C. Fan, C. Zhang, X. He, Y. He, An overview on limitations of TiO_2-based particles for photocatalytic degradation of organic pollutants and the corresponding countermeasures, Water Res. 79 (2015) 128–146.

[19] K.M. Lee, C.W. Lai, K.S. Ngai, J.C. Juan, Recent developments of zinc oxide based photocatalyst in water treatment technology: a review, Water Res. 88 (2016) 428–448.

[20] S. Rehman, R. Ullah, A. Butt, N. Gohar, Strategies of making TiO_2 and ZnO visible light active, J. Hard Mater. 170 (2–3) (2009) 560–569.

[21] K. Davis, R. Yarbrough, M. Froeschle, J. White, H. Rathnayake, Band gap engineered zinc oxide nanostructures via a sol–gel synthesis of solvent driven shape-controlled crystal growth, RSC Adv. 9 (26) (2019) 14638–14648.

[22] Y. Tang, H. Zhou, K. Zhang, J. Ding, T. Fan, D. Zhang, Visible-light-active ZnO via oxygen vacancy manipulation for efficient formaldehyde photodegradation, Chem. Eng. J. 262 (2015) 260–267.

[23] C. Dette, M.A. Pérez-Osorio, C.S. Kley, P. Punke, C.E. Patrick, P. Jacobson, F. Giustino, S.J. Jung, K. Kern, TiO_2 anatase with a bandgap in the visible region, Nano Lett. 14 (11) (2014) 6533–6538.

[24] S. Hotchandani, P.V. Kamat, Photoelectrochemistry of semiconductor ZnO particulate films, J. Electrochem. Soc. 139 (6) (1992) 1630.

[25] X. Li, Z. Hu, J. Liu, D. Li, X. Zhang, J. Chen, J. Fang, Ga doped ZnO photonic crystals with enhanced photocatalytic activity and its reaction mechanism, Appl. Catal. B 195 (2016) 29–38.

[26] S.P. Pitre, T.P. Yoon, J.C. Scaiano, Titanium dioxide visible light photocatalysis: surface association enables photocatalysis with visible light irradiation, Chem. Commun. 53 (31) (2017) 4335–4338.

[27] J. Liu, H. Zhao, M. Wu, B. Van der Schueren, Y. Li, O. Deparis, J. Ye, G.A. Ozin, T. Hasan, B.-L. Su, Slow photons for photocatalysis and photovoltaics, Adv. Mater. 29 (17) (2017) 1605349.

[28] M. Diepens, P. Gijsman, Influence of light intensity on the photodegradation of bisphenol A polycarbonate, Polym. Degrad. Stab. 94 (1) (2009) 34–38.

[29] M. Tanveer, G.T. Guyer, Solar assisted photo degradation of wastewater by compound parabolic collectors: Review of design and operational parameters, Renew. Sustain. Energy Rev. 24 (2013) 534–543.

[30] A.M. Khaksar, S. Nazif, A. Taebi, E. Shahghasemi, Treatment of phenol in petrochemical wastewater considering turbidity factor by backlight cascade photocatalytic reactor, J. Photochem. Photobiol. A: Chem. 348 (2017) 161–167.

[31] J.V. Vaghasiya, K.K. Sonigara, L. Suresh, M. Panahandeh-Fard, S.S. Soni, S.C. Tan, Efficient power generating devices utilizing low intensity indoor lights via non-radiative energy transfer mechanism from organic ionic redox couples, Nano Energy 60 (2019) 457–466.

[32] M.M. Kandy, V.G. Gaikar, Enhanced photocatalytic reduction of CO_2 using cds/Mn_2O_3 nanocomposite photocatalysts on porous anodic alumina support with solar concentrators, Renew. Energy 139 (2019) 915–923.

[33] C. Zhang, N. Liu, J. Ming, A. Sharma, Q. Ma, Z. Liu, G. Chen, Y. Yang, Development of a novel solar energy controllable linear fresnel photoreactor (LFP) for high-efficiency photocatalytic wastewater treatment under actual weather, Water Res. 208 (2022) 117880.

[34] M. Nakano, Y. Nishiyama, H. Tanimoto, T. Morimoto, K. Kakiuchi, Remarkable improvement of organic photoreaction efficiency in the flow microreactor by the slug flow condition using water, Org. Process Res. Dev. 20 (9) (2016) 1626–1632.

[35] W. Li, S. Wu, H. Zhang, X. Zhang, J. Zhuang, C. Hu, Y. Liu, B. Lei, L. Ma, X. Wang, Enhanced biological photosynthetic efficiency using light-harvesting engineering with dual-emissive carbon dots, Adv. Funct. Mater. 28 (44) (2018) 1804004.

[36] J.-W.F. Zijffers, S. Salim, M. Janssen, J. Tramper, R.H. Wijffels, Capturing sunlight into a photobioreactor: Ray tracing simulations of the propagation of light from capture to distribution into the reactor, Chem. Eng. J. 145 (2) (2008) 316–327.

[37] D. Daly, Microlens Arrays, CRC Press, 2000.

[38] L. Commander, S. Day, D. Selviah, Variable focal length microlenses, Opt. Commun. 177 (1–6) (2000) 157–170.

[39] J. Seo, L.P. Lee, Disposable integrated microfluidics with self-aligned planar microlenses, Sensors Actuators B 99 (2–3) (2004) 615–622.

[40] L. Dong, A.K. Agarwal, D.J. Beebe, H. Jiang, Adaptive liquid microlenses activated by stimuli-responsive hydrogels, Nature 442 (7102) (2006) 551–554.

[41] J.Y. Lee, B.H. Hong, W.Y. Kim, S.K. Min, Y. Kim, M.V. Jouravlev, R. Bose, K.S. Kim, I.-C. Hwang, L.J. Kaufman, et al., Near-field focusing and magnification through self-assembled nanoscale spherical lenses, Nature 460 (7254) (2009) 498–501.

[42] B. Dyett, Q. Zhang, Q. Xu, X. Wang, X. Zhang, Extraordinary focusing effect of surface nanolenses in total internal reflection mode, ACS Cent. Sci. 4 (11) (2018) 1511–1519.

[43] Y. Bao, W.J. Lee, J.Z.Y. Seow, H. Hara, Y.N. Liang, H. Feng, J.Z. Xu, T.-T. Lim, X. Hu, One-step block copolymer templated synthesis of bismuth oxybromide for bisphenol a degradation: an extended study from photocatalysis to chemical oxidation, ACS ES T Water 1 (4) (2021) 837–846.

[44] X. Wu, C. Fang, W. Xu, D. Zhang, Bioinspired compound eyes for diffused light-harvesting application, ACS Appl. Mater. Interfaces (2022).

[45] Y. Huang, Y. Qin, P. Tu, Q. Zhang, M. Zhao, Z. Yang, High fill factor microlens array fabrication using direct laser writing and its application in wavefront detection, Opt. Lett. 45 (16) (2020) 4460–4463.

[46] J.-G. Hua, H. Ren, A. Jia, Z.-N. Tian, L. Wang, S. Juodkazis, Q.-D. Chen, H.-B. Sun, Convex silica microlens arrays via femtosecond laser writing, Opt. Lett. 45 (3) (2020) 636–639.

[47] S. Moore, J. Gomez, D. Lek, B.H. You, N. Kim, I.-H. Song, Experimental study of polymer microlens fabrication using partial-filling hot embossing technique, Microelectron. Eng. 162 (2016) 57–62.

[48] N. Jürgensen, B. Fritz, A. Mertens, J.-N. Tisserant, M. Kolle, G. Gomard, G. Hernandez-Sosa, A single-step hot embossing process for integration of microlens arrays in biodegradable substrates for improved light extraction of light-emitting devices, Adv. Mater. Technol. 6 (2) (2021) 1900933.

[49] M.V. Kunnavakkam, F. Houlihan, M. Schlax, J. Liddle, P. Kolodner, O. Nalamasu, J. Rogers, Low-cost, low-loss microlens arrays fabricated by soft-lithography replication process, Appl. Phys. Lett. 82 (8) (2003) 1152–1154.

[50] M. Li, Q. Yang, H. Bian, T. Yang, X. Hou, F. Chen, Microlens arrays enable variable-focus imaging, Opt. Laser Technol. 153 (2022) 108260.

[51] J. Liu, M.-J. Chang, Y. Ai, H.-L. Zhang, Y. Chen, Fabrication of microlens arrays by localized hydrolysis in water droplet microreactors, ACS Appl. Mater. Interfaces 5 (6) (2013) 2214–2219.

[52] L. Mei, C. Qu, Z. Xu, G. Wang, J. Zhang, X. Guo, Y. Peng, Facile fabrication of microlens array on encapsulation layer for enhancing angular color uniformity of color-mixed light-emitting diodes, Opt. Laser Technol. 142 (2021) 107227.

[53] X. Zhang, Z. Lu, H. Tan, L. Bao, Y. He, C. Sun, D. Lohse, Formation of surface nanodroplets under controlled flow conditions, Proc. Natl. Acad. Sci. 112 (30) (2015) 9253–9257.

[54] X. Zhang, J. Ren, H. Yang, Y. He, J. Tan, G.G. Qiao, From transient nanodroplets to permanent nanolenses, Soft Matter 8 (16) (2012) 4314–4317.

[55] L. Bao, A.R. Rezk, L.Y. Yeo, X. Zhang, Highly ordered arrays of femtoliter surface droplets, Small 11 (37) (2015) 4850–4855.

[56] P.D. Dongare, A. Alabastri, O. Neumann, P. Nordlander, N.J. Halas, Solar thermal desalination as a nonlinear optical process, Proc. Natl. Acad. Sci. 116 (27) (2019) 13182–13187.

[57] Q. Lu, Q. Xu, J. Meng, Z.T. How, P. Chelme-Ayala, X. Wang, M. Gamal El-Din, X. Zhang, Surface microlenses for much more efficient photodegradation in water treatment, ACS ES T Water 2 (4) (2022) 644–657.

[58] X. Luo, Y. Zhan, Y. Huang, L. Yang, X. Tu, S. Luo, Removal of water-soluble acid dyes from water environment using a novel magnetic molecularly imprinted polymer, J. Hard Mater. 187 (1–3) (2011) 274–282.

[59] S. Ren, Q. Li, J. Wang, B. Fan, J. Bai, Y. Peng, S. Li, D. Han, J. Wu, J. Wang, et al., Development of a fast and ultrasensitive black phosphorus-based colorimetric/photothermal dual-readout immunochromatography for determination of norfloxacin in tap water and river water, J. Hard Mater. 402 (2021) 123781.

[60] S. Bahnmüller, U. von Gunten, S. Canonica, Sunlight-induced transformation of sulfadiazine and sulfamethoxazole in surface waters and wastewater effluents, Water Res. 57 (2014) 183–192.

[61] X.H. Zhang, W. Ducker, Formation of interfacial nanodroplets through changes in solvent quality, Langmuir 23 (25) (2007) 12478–12480.

[62] G. Tian, H. Fu, L. Jing, C. Tian, Synthesis and photocatalytic activity of stable nanocrystalline TiO_2 with high crystallinity and large surface area, J. Hard Mater. 161 (2–3) (2009) 1122–1130.

[63] W. Chen, Q. Liu, S. Tian, X. Zhao, Exposed facet dependent stability of ZnO micro/nano crystals as a photocatalyst, Appl. Surf. Sci. 470 (2019) 807–816.

[64] J. Qian, G.F. Arends, X. Zhang, Surface nanodroplets: formation, dissolution, and applications, Langmuir 35 (39) (2019) 12583–12596.

[65] L. Lei, J. Li, H. Yu, L. Bao, S. Peng, X. Zhang, Formation, growth and applications of femtoliter droplets on a microlens, Phys. Chem. Chem. Phys. 20 (6) (2018) 4226–4237.

[66] P. Makuła, M. Pacia, W. Macyk, How to correctly determine the band gap energy of modified semiconductor photocatalysts based on UV–Vis spectra, J. Phys. Chem. Lett. 9 (23) (2018) 6814–6817.

[67] A. Zhang, Y. Fang, Influence of adsorption orientation of methyl orange on silver colloids by Raman and fluorescence spectroscopy: pH effect, Chem. Phys. 331 (1) (2006) 55–60.

[68] L. Saikia, D. Bhuyan, M. Saikia, B. Malakar, D.K. Dutta, P. Sengupta, Photocatalytic performance of ZnO nanomaterials for self sensitized degradation of malachite green dye under solar light, Appl. Catal. A: Gen. 490 (2015) 42–49.

[69] S. Ahluwalia, N.T. Prakash, R. Prakash, B. Pal, Improved degradation of methyl orange dye using bio-co-catalyst Se nanoparticles impregnated ZnS photocatalyst under UV irradiation, Chem. Eng. J. 306 (2016) 1041–1048.

[70] A. Lipovsky, Z. Tzitrinovich, H. Friedmann, G. Applerot, A. Gedanken, R. Lubart, EPR study of visible light-induced ROS generation by nanoparticles of ZnO, J. Phys. Chem. C 113 (36) (2009) 15997–16001.

[71] X. Li, P. Zhang, L. Jin, T. Shao, Z. Li, J. Cao, Efficient photocatalytic decomposition of perfluorooctanoic acid by indium oxide and its mechanism, Environ. Sci. Technol. 46 (10) (2012) 5528–5534.

[72] C.S. Turchi, D.F. Ollis, Photocatalytic degradation of organic water contaminants: mechanisms involving hydroxyl radical attack, J. Catalysis 122 (1) (1990) 178–192.

[73] R.G. Zepp, D.M. Cline, Rates of direct photolysis in aquatic environment, Environ. Sci. Technol. 11 (4) (1977) 359–366.

[74] M. Persico, G. Granucci, Photochemistry: A Modern Theoretical Perspective, Springer, 2018.

[75] S. Ahmed, M. Rasul, R. Brown, M. Hashib, Influence of parameters on the heterogeneous photocatalytic degradation of pesticides and phenolic contaminants in wastewater: a short review, J. Environ. Manag. 92 (3) (2011) 311–330.

[76] A. Rafiq, M. Ikram, S. Ali, F. Niaz, M. Khan, Q. Khan, M. Maqbool, Photocatalytic degradation of dyes using semiconductor photocatalysts to clean industrial water pollution, J. Ind. Eng. Chem. 97 (2021) 111–128.

[77] Z. Wang, W. Ma, C. Chen, H. Ji, J. Zhao, Probing paramagnetic species in titania-based heterogeneous photocatalysis by electron spin resonance (ESR) spectroscopy—a mini review, Chem. Eng. J. 170 (2–3) (2011) 353–362.

[78] Y. Kim, H.M. Hwang, L. Wang, I. Kim, Y. Yoon, H. Lee, Solar-light photocatalytic disinfection using crystalline/amorphous low energy bandgap reduced TiO_2, Sci. Rep. 6 (1) (2016) 1–10.

[79] K. Vinodgopal, D.E. Wynkoop, P.V. Kamat, Environmental photochemistry on semiconductor surfaces: photosensitized degradation of a textile azo dye, acid orange 7, on TiO_2 particles using visible light, Environ. Sci. Technol. 30 (5) (1996) 1660–1666.

[80] X. Yan, T. Ohno, K. Nishijima, R. Abe, B. Ohtani, Is methylene blue an appropriate substrate for a photocatalytic activity test? A study with visible-light responsive titania, Chem. Phys. Lett. 429 (4–6) (2006) 606–610.

[81] M. Martín-Sómer, C. Pablos, R. van Grieken, J. Marugán, Influence of light distribution on the performance of photocatalytic reactors: LED vs mercury lamps, Appl. Catal. B 215 (2017) 1–7.

[82] S. Selvaraj, B. Palanivel, S. Patrick, M. Krishna Mohan, M. Navaneethan, S. Ponnusamy, C. Muthamizhchelvan, Effect of Sr doping in ZnO microspheres for solar light-driven photodegradation of organic pollutants, J. Mater. Sci., Mater. Electron. 33 (11) (2022) 8777–8788.

[83] N.P. Xekoukoulotakis, C. Drosou, C. Brebou, E. Chatzisymeon, E. Hapeshi, D. Fatta-Kassinos, D. Mantzavinos, Kinetics of UV-A/TiO_2 photocatalytic degradation and mineralization of the antibiotic sulfamethoxazole in aqueous matrices, Catal. Today 161 (1) (2011) 163–168.